第 43 卷 第 1 期/2023 年 1 月/光学学报 研究论文

光学学报

# FP腔与MZI级联的三参量同时测量的光纤传感器

彭敏，鲁志琪，刘昌宁*

湖北师范大学物理与电子科学学院，湖北 黄石 435002

**摘要** 制作了敏感材料修饰的拉锥光纤与微腔级联的多参量光纤传感器，并用实验研究了其应变、温度和湿度特性。所提微腔由飞秒激光划线放电形成，并对其进行拉锥。传感器的反射光谱干涉峰对应变的变化敏感，实验结果表明应变灵敏度为4.8 pm/με。然而，该结构对温度与湿度均不敏感，在该结构的锥部涂覆了掺入石墨烯量子点的聚乙烯醇之后，温度和湿度的灵敏度明显提升，此时最大温度灵敏度为20.4 pm/℃，最大相对湿度灵敏度最大为14.6 pm/%。对Dip1、Dip2、Dip3进行分析，再利用三阶矩阵消除交叉敏感，能够同时测量应变、温度和湿度。

**关键词** 光纤光学；光纤传感器；应变；温度；相对湿度；石墨烯量子点；聚乙烯醇

**中图分类号** O439 **文献标志码** A **DOI**：10.3788/AOS221193

## 1 引 言

光纤传感器不仅具有重量轻、尺寸小和抗电磁干扰等优点，而且使用的光缆也比电子传感器的电缆有更低的热损耗或更高的数据带宽[1-2]。根据原理分类，光纤传感器有许多不同种类：光纤布拉格光栅（FBG）应用广泛但光栅刻写较为复杂；基于特种光纤的传感器价格较为昂贵，熔接程序复杂；干涉仪型光纤传感器，包括法布里-珀罗干涉仪（FPI）、马赫-曾德尔干涉仪（MZI）和迈克耳孙干涉仪（MI）等，其中MZI和FPI应用较为广泛[3-4]。MZI有着耦合效率较高、易于对准和成本低的优点[5-6]，其中基于锥形结构的MZI传感器具有高灵敏度、低损耗、大倏逝场和快速响应等优点。光纤应变传感器在航空航天、纳米技术等领域中有广泛的应用[7]，如：Dong等[8]提出了基于锥形空芯的高灵敏度应变光纤传感器，其应变灵敏度为2.7 pm/με；Dong等[9]提出了基于全光纤MZI的应变传感器，其灵敏度为−2.21 pm/με。湿度与温度是环境测量的两个重要参数，而石英光纤对于温度与湿度通常是传而不感，对于敏感材料是感而不传。为了提高传感器的灵敏度，通常会在传感头上涂覆敏感材料，最终达到既能感又能传的效果。湿敏材料如聚乙烯醇（PVA）是高度亲水性材料，其厚度和折射率可通过水蒸气改变，并且易涂覆在光纤上[10-12]。另外，石墨烯以其优异的性能吸引了大量研究人员的关注，在光纤传感器中的应用变得异常丰富[13-20]。石墨烯量子点（GQDs）是一种由单层或多层石墨烯组成的新型碳纳米材料，同时具有石墨烯和量子点的特性，其优异的热光性能使其在传感器、生物医学领域的研究中受到了越来越多的关注[21]，如：Zhao等[22-23]利用GQDs的光致发光特性制作了基于空芯光纤封装GQDs溶液的荧光温度传感器和基于空芯光纤填充的GQDs-PVA的相对湿度（RH）传感器；Wang等[24]制作了GQDs填充FPI的光纤湿度传感器。在许多复杂的环境中，仅测量一个参数已经不能满足人们的需求，温度与折射率、温度与压力等双参量的测量越来越多[25-29]。本文主要利用飞秒激光划线和光纤熔接机放电的方法制作出了MZI与FPI级联构成的光纤传感器件。传统的级联需要通过两段干涉仪或者光纤光栅进行拼接[30-32]，而本文中的传感器不需要额外的拼接过程，只需在光纤上利用飞秒激光刻线进行放电产生气泡，再拉锥形成器件，结构更加紧凑，整个传感区域长度不到400 μm。另外，利用飞秒激光在任意位置划线均可精准地产生气泡，不需要额外加上液体进行熔接再产生FP腔。所设计的传感器的应变灵敏度最高可达4.8 pm/με，对温度、湿度均不敏感，在涂覆GQDs-PVA之后，温度灵敏度最高可达20.4 pm/℃，相对湿度灵敏度最高为14.6 pm/%，选取三个波谷Dip1、Dip2、Dip3进行分析，利用三阶矩阵消除交叉敏感后能够实现三参量同时测量。

**收稿日期**：2022-05-24；**修回日期**：2022-06-20；**录用日期**：2022-07-04；**网络首发日期**：2022-07-14

**基金项目**：湖北省高等学校优秀中青年科技创新团队计划（T2020014，T2021010）、湖北师范大学研究生创新科研基金（20220501）

**通信作者**：*liusir1001@163.com

## 2 光纤传感器结构制作与原理分析

### 2.1 传感器结构的制作

本实验所用的光纤熔接机（FSM-100P+）由日本Fujikura公司生产，单模光纤（SMF）由长飞光纤光缆股份有限公司生产，其芯径和包层直径分别为9 μm和125 μm。如图1(a)所示，飞秒激光器由相干公司生产，重复频率为1 kHz，脉冲宽度为35 fs，实验所使用的激光能量为1.2 μJ，用放大倍数为50、数值孔径为0.7的OLYMPUS物镜聚焦飞秒激光到SMF纤芯上，运行程序在轴向方向刻线，控制刻线长度为45 μm，如图1(b)所示。然后，用光纤熔接机对准刻线的中心位置进行放电，熔接机的放电电流和放电时间分别设置为20 mA和1500 ms，瞬间放电使光纤内产生气泡，如图1(c)所示，其宽度为82 μm、长度为129 μm。

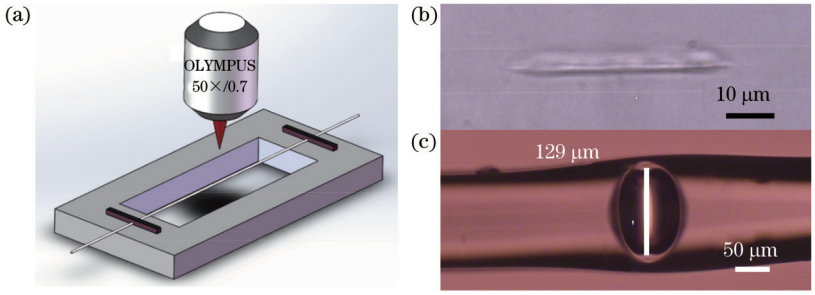


图1 FP微腔的制作。(a)飞秒激光加工示意图；(b)飞秒激光刻线的显微镜图；(c) FP微气泡

Fig. 1 Fabrication of FP micro-cavity. (a) Schematic diagram of femtosecond laser processing; (b) microscope diagram of femtosecond laser inscribed line; (c) FP microbubble

如图2(a)所示，将SMF拉锥得到MZI，锥区直径越小，传感器倏逝场越强，此时传感器对周围环境越敏感，但锥部直径过小容易导致测量范围变小，锥部直径太大又会导致灵敏度不够，拉锥到40 μm左右是一个相对合理的直径，既能保持器件对环境敏感，又能保证较大的测量范围，此时MZI的锥部区域被拉伸至277 μm，MZI与微气泡FP腔级联可构成所需的传感器件。

如图2(b)所示，镀膜之后锥部的束腰直径为48 μm，可知镀膜厚度为4 μm。实验所使用的GQDs为苏州碳丰石墨烯科技有限公司生产，PVA的生产厂家是国药集团化学试剂有限公司。取GQDs约5 mg，PVA约100 mg，混合均匀后加入100 mL纯净水，再加热到95 ℃，用磁力搅拌机作用1 h，使之搅拌均匀，从而得到GQDs-PVA溶液。用注射器取1.5 mL溶液均匀涂覆在光纤锥部，将传感器放入真空干燥箱内，设置干燥箱参数为80 ℃、30 min，GQDs-PVA溶液中的溶剂蒸发后可以发现有一层薄膜附着在传感器锥部，其主要成分是PVA和GQDs。将薄膜放在扫描电子显微镜（SEM）下观察，可知PVA膜中GQDs的尺寸与分布情况，如图2(c)所示。

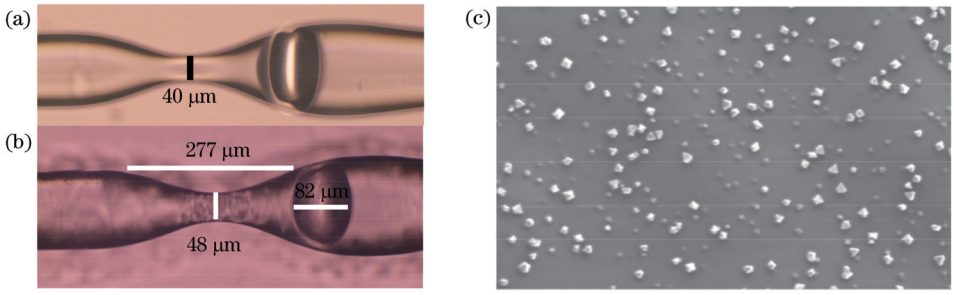


图2 传感器实物图。(a)镀膜前的传感器；(b)镀膜后的传感器；(c) SEM测得的GQDs-PVA

Fig. 2 Physical diagram of sensor. (a) Sensor before coating; (b) sensor after coating; (c) GQDs-PVA measured by SEM

图3(a)为涂覆GQDs-PVA后传感器的初始光谱，后续实验将对波谷Dip1、Dip2、Dip3进行观察与分析。对初始光谱进行快速傅里叶变换后得到传感器的空间频谱，如图3(b)所示，对干涉起主要作用的两个频率分别为0.03418 $nm^{-1}$和0.06836 $nm^{-1}$，它们是由FPI与MZI分别起作用而形成的不同频率。

### 2.2 传感原理简单分析

图4为传感器光路的示意图，传感器由MZI和FPI级联而成。MZI是一段锥形光纤，光从锥形光纤一端输入，由于纤芯的直径在变小，故部分高阶模会在包层中传输，部分纤芯模会沿着纤芯传输。FPI是一个气泡，经过MZI后的输入光先后从气泡的两个反射面反射回来，再返回到MZI中，最终形成干涉的输出光。

相位差是由不同模式之间的光程差形成的，MZI形成的相位差$\varphi_1$和FPI形成的相位差$\varphi_2$的计算公式为

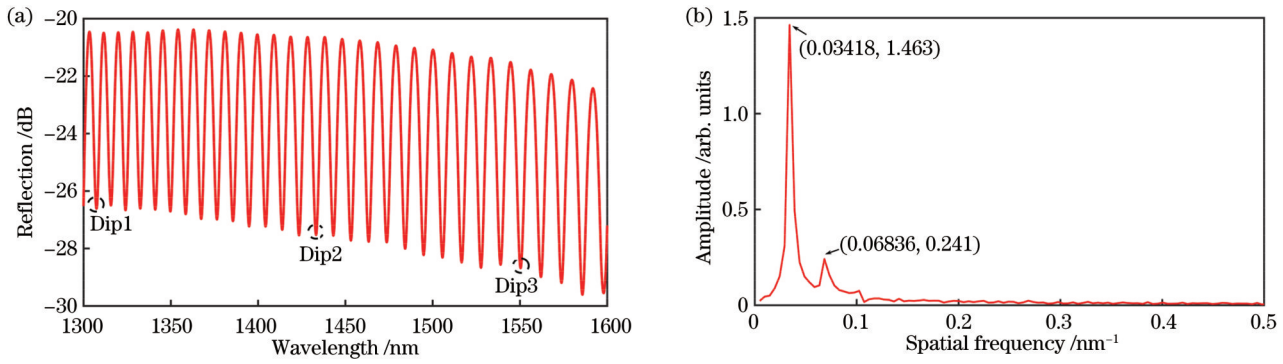


图 3　传感器初始反射光谱图与空间频谱图。(a)初始反射光谱图;(b)空间频谱图

Fig. 3　Initial reflectance spectrum and spatial spectrum of sensor. (a) Initial reflectance spectrogram; (b) spatial spectrum

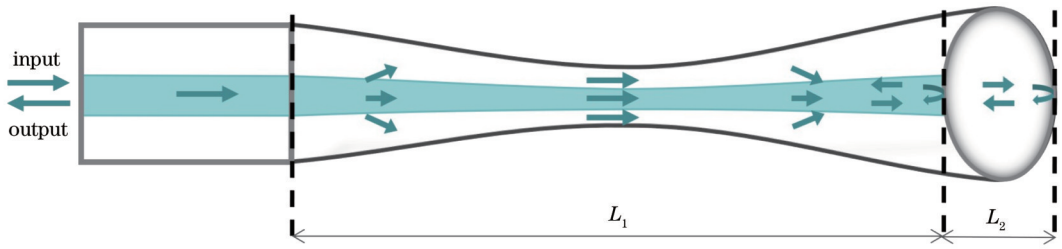


图 4　传感器光路示意图

Fig. 4　Schematic diagram of sensor optical path

$$\varphi_1=\frac{2\pi(n_{co}^{eff}-n_{cl}^{eff})}{\lambda}L_1=\frac{2\pi\Delta n_{eff}}{\lambda}L_1\,, \tag{1}$$

$$\varphi_2=\frac{4\pi L_2 n_{air}}{\lambda}\,, \tag{2}$$

式中:$n_{cl}^{eff}$为包层模的有效折射率;$n_{co}^{eff}$为纤芯的有效折射率;$\Delta n_{eff}$为纤芯模与包层模的有效折射率之差;$n_{air}$为FPI的腔内折射率;$L_1$为MZI的锥部长度;$L_2$为FPI的腔长;$\lambda$为波长。当$m$、$n$取整数时,干涉仪的谐振峰波长分别为

$$\lambda_m=\frac{2L_1\Delta n_{eff}}{2m+1}, \tag{3}$$

$$\lambda_n=\frac{4L_2 n_{air}}{2n+1}。 \tag{4}$$

当应力$\xi=\Delta L/L$($\Delta L$为应变平台的移动距离,$L$为应变平台初始距离)作用于器件时,FPI的腔长$L_2$和MZI的锥部长度$L_1$均会发生变化,并且折射率也会产生变化,最终会导致谱线发生偏移,其中FPI腔内空气折射率的变化可以忽略不计。当应力作用时,干涉光谱中谐振峰的波长灵敏度可以表示为

$$S_F=\frac{\Delta\lambda_m}{\Delta\xi}+\frac{\Delta\lambda_n}{\Delta\xi}=\frac{2}{2m+1}\left[\Delta_{eff}\frac{dL_1}{d\xi}+L_1\left(\frac{dn_{co}^{eff}}{d\xi}-\frac{dn_{cl}^{eff}}{d\xi}\right)\right]+\frac{4}{2n+1}n_{air}\frac{dL_2}{d\xi}\,, \tag{5}$$

式中:$\Delta\lambda_m$为MZI的干涉谱波长的变化量;$\Delta\lambda_n$为FPI的干涉谱波长的变化量;$\Delta\xi$为应变的变化量;$\Delta_{eff}$为有效折射率差。

$p_{co}^{eff}$和$p_{cl}^{eff}$分别为纤芯和包层的有效弹光系数,且满足

$$p_{co}^{eff}=-\frac{1}{n_{co}^{eff}}\frac{dn_{co}^{eff}}{d\xi}\;p_{cl}^{eff}=-\frac{1}{n_{cl}^{eff}}\frac{dn_{cl}^{eff}}{d\xi}。 \tag{6}$$

当应力发生变化时,灵敏度可以简化为

$$S_F=\frac{2L_1}{2m+1}\left(\Delta_{eff}+p_{cl}^{eff}n_{cl}^{eff}-p_{co}^{eff}n_{co}^{eff}\right)+\frac{4L_2}{2n+1}n_{air}。 \tag{7}$$

在温度实验中,由于石墨烯的热效应较强,故GQDs会导致光谱产生漂移。当传感器的温度发生变化时,MZI的折射率和腔长均会产生变化,而FPI腔里面是空气,故对于FPI腔只需要考虑热膨胀而引起的腔长变化。通过观察不同温度的漂移规律,可以测得对应的温度灵敏度,其公式可表示为

$$S=S_{T\text{-}MZI}+S_{T\text{-}FPI}=\frac{\Delta\lambda_m}{\Delta T}+\frac{\Delta\lambda_n}{\Delta T}=\lambda_m\left[\frac{dL_1}{L_1dT}+\frac{1}{\Delta n_{eff}}\left(\frac{d\Delta_{co}^{eff}}{dT}-\frac{d\Delta_{cl}^{eff}}{dT}\right)\right]+\lambda_n\frac{dL_2}{L_2dT}, \tag{8}$$

式中:$S_{T\text{-}MZI}$为MZI的温度灵敏度;$S_{T\text{-}FPI}$为FPI的温度灵敏度;$\Delta T$为温度变化量;$\Delta_{co}^{eff}$为纤芯的有效折射率变化量;$\Delta_{cl}^{eff}$为包层的有效折射率变化量;$\frac{dL_1}{L_1dT}$和$\frac{dL_2}{L_2dT}$为热膨胀系数,$\frac{d\Delta_{co}^{eff}}{dT}$和$\frac{d\Delta_{cl}^{eff}}{dT}$为热光系数。热膨胀系数和热光系数分别为$5.5\times10^{-7}$ m/(m·℃)和$1.28\times10^{-5}$ RIU/℃(RIU为折射率单位)[33]。

PVA的折射率约为1.52,纯净水的折射率约为

1.33，在MZI的锥部涂覆GQDs-PVA之后，相对湿度（$V_{RH}$）发生变化，GQDs-PVA的折射率也会发生变化，这会导致两束干涉光的有效折射率之差发生变化。FPI是一个封闭的结构，湿度的变化并不会改变腔内折射率，腔长也不会改变。FPI的灵敏度可表示为

$$S_{RH}=\frac{\Delta\lambda_m}{\Delta V_{RH}}=\frac{\lambda_m}{L_1\Delta_{eff}}\left[\Delta_{eff}\mathrm{d}L_1+\frac{L_1}{\mathrm{d}V_{RH}}\left(\mathrm{d}\Delta_{co}^{eff}-\mathrm{d}\Delta_{cl}^{eff}\right)\right],\tag{9}$$

式中：$\Delta V_{RH}$为相对湿度的变化量。湿度的变化也不会引起MZI的腔长变化，芯层的折射率也不会改变，式(9)可以简化为

$$S_{RH}=\frac{2L_1}{2m+1}\frac{\mathrm{d}\Delta_{cl}^{eff}}{\mathrm{d}V_{RH}}。\tag{10}$$

从式(7)、式(8)和式(10)可知，反射光谱中的干涉峰波长对应力、温度、湿度的响应度不同。因此，可以通过灵敏度系数构建三阶矩阵，实现三参量的同时测量。

## 3　实验结果与分析

图5展示了应变、温度、湿度的实验装置图，以及可编程的温度湿度实验箱。实验箱温度测量范围为20～100 ℃，测量的精度为±0.1 ℃，相对湿度测量范围为10%～95%，测量的精度为±0.1%。所采用的宽带光源（BBS）是型号为FL-ASE-EB-D-2-2-FC/APC的自发辐射光源，光谱的范围为1250～1650 nm。所采用的光谱分析仪（OSA）由YOKOGAWA生产，型号为AQ6370D，其测量范围为600～1700 nm，精度为±0.1 nm。光从BBS输出，经耦合器传输至传感器之后，反射光再由耦合器传输到OSA中，然后进行实验并提取数据进行分析。

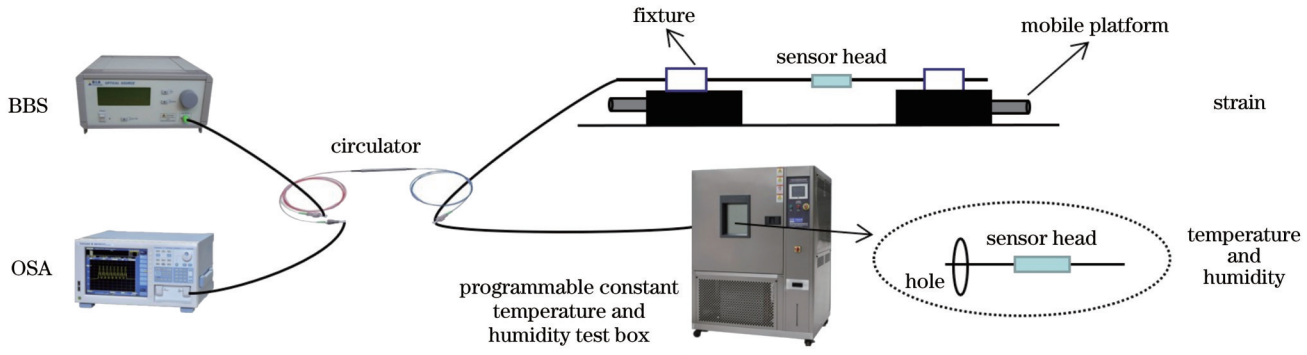


图5　实验装置图

Fig. 5　Diagram of experimental setup

### 3.1　应变传感实验

在进行应变实验时，将传感器两端拉直固定在应变平台上，设置应变平台初始距离$L$为25 cm，旋转右端应变平台上的千分尺，每转动一格右移10 μm，设为$\Delta L$。利用轴向应变变化公式$\varepsilon=\Delta L/L$可得轴向应变间隔为40 με，即每隔40 με记录一次反射光谱，旋转15次，轴向应变变化范围为0～600 με。实验结果表明，随着轴向应变的增大，反射光谱的谐振峰整体向右漂移。波谷Dip1(1307 nm)的反射光谱变化图和线性拟合图如图6(a)、(d)所示，波谷Dip2(1432 nm)的反射光谱变化图和线性拟合图如图6(b)、(e)所示，波谷Dip3(1550 nm)的反射光谱变化图和线性拟合图如图6(c)、(f)示，分别分析其漂移规律，可得轴向应变灵敏度分别为4.0 pm/με、4.3 pm/με、4.8 pm/με，线性拟合度分别为0.9993、0.9995、0.9996，三者线性度均较高。

### 3.2　温度传感实验

在进行温度实验时，设定相对湿度40%不变，温度从24～80 ℃逐步上升，间隔4 ℃为一组，并且稳定15 min左右再记录反射谱，总共记录了15组数据。如图7所示，镀GQDs-PVA薄膜之前，随着温度的上升，波长漂移几乎为零。然而，镀GQDs-PVA之后：选Dip1观察其光谱变化，分析得到此时温度灵敏度为16.6 pm/℃，线性拟合度为0.9857，如图8(a)、(d)所示；Dip2的温度灵敏度为18.5 pm/℃，线性拟合度为0.9859，如图8(b)、(e)所示；Dip3的温度灵敏度为20.4 pm/℃，线性拟合度为0.9867，如图8(c)、(f)所示。

### 3.3　湿度传感实验

在进行湿度实验时，将传感器放至恒温恒湿试验箱中，该传感器的一端通过试验箱的小孔连接到环形器，环形器的另外两端分别连接至BBS与OSA。设定温度为40 ℃并保持不变，相对湿度从40%逐步变化至70%，间隔为5%，每次稳定15 min左右后记录一次数据，共得到7组数据。石英玻璃对湿度并不敏感，镀膜之前反射光谱的波长不产生漂移，涂覆GQDs-PVA之后，反射谱光谱的波长随着湿度的上升整体红移：波谷Dip1的中心波长与湿度有很好的线性关系，线性拟合度为0.9889，相对湿度灵敏度为12.6 pm/%，如图9(a)、(d)所示；波谷Dip2的相对湿度灵敏度为

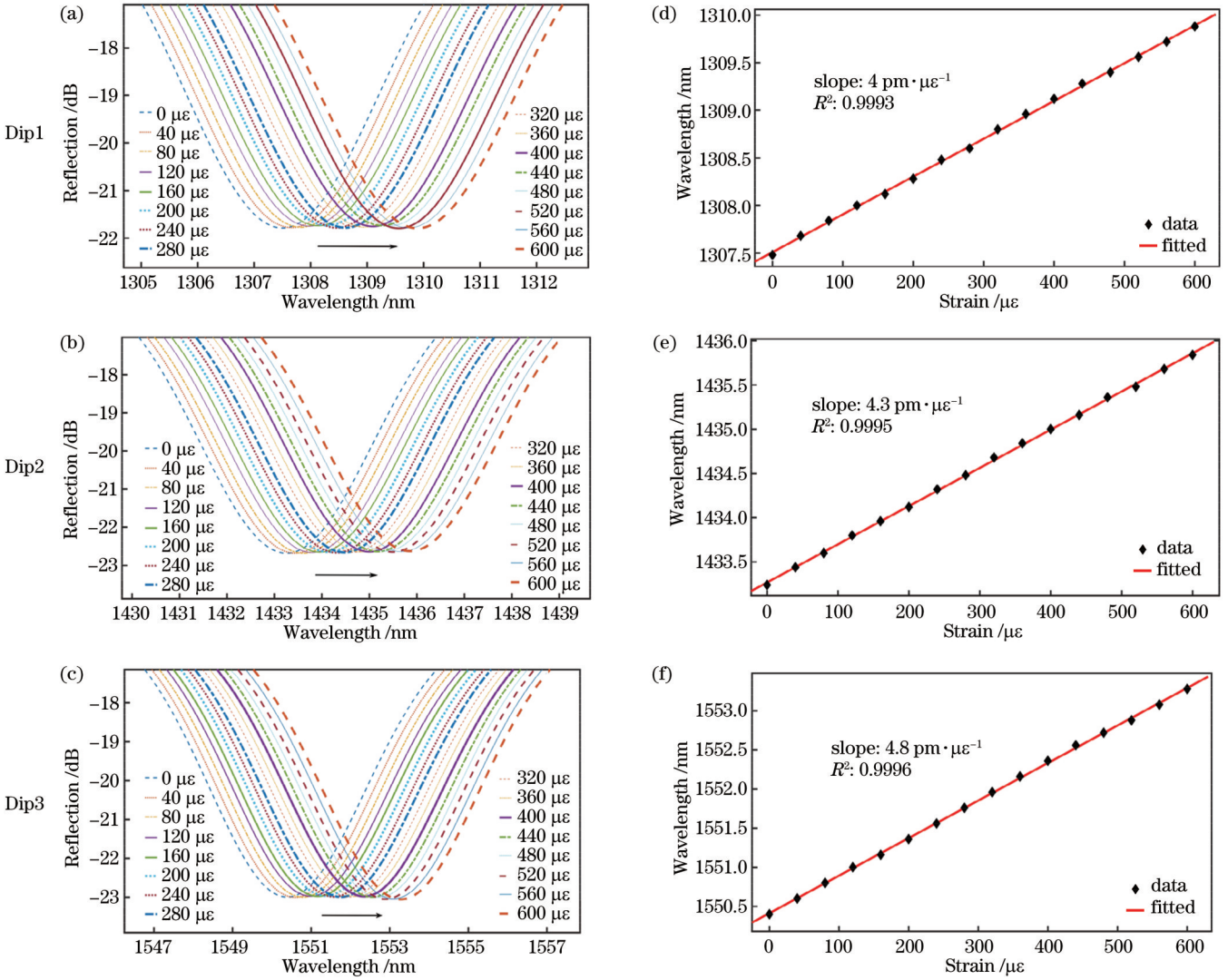


图 6　应变实验的反射光谱变化图与线性拟合图。(a)～(c)反射光谱变化图；(d)～(f)线性拟合图

Fig. 6　Reflection spectrum variation diagram and linear fitting diagram of strain experiment. (a)-(c) Reflection spectrum variation diagram; (d)-(f) linear fitting diagram

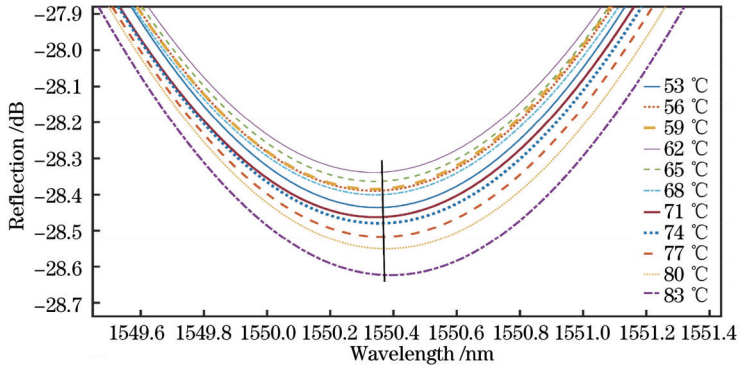


图 7　镀膜前温度实验的反射光谱

Fig. 7　Reflection spectra of temperature test before coating

13.5 pm/%，线性拟合度为 0.9652，如图 9(b)、(e)所示；波谷 Dip3 的相对湿度灵敏度为 14.6 pm/%，线性拟合度为 0.9863，如图 9(c)、(f)所示。

为了消除三参量之间的交叉敏感，当外界的应变、温度和湿度变化时，三者之间的关系可描述为

$$\begin{cases}\Delta\lambda_1 = K_{S_1}\Delta\varepsilon + K_{T_1}\Delta T + K_{H_1}\Delta H \\ \Delta\lambda_2 = K_{S_2}\Delta\varepsilon + K_{T_2}\Delta T + K_{H_2}\Delta H \\ \Delta\lambda_3 = K_{S_3}\Delta\varepsilon + K_{T_3}\Delta T + K_{H_3}\Delta H\end{cases}, \tag{11}$$

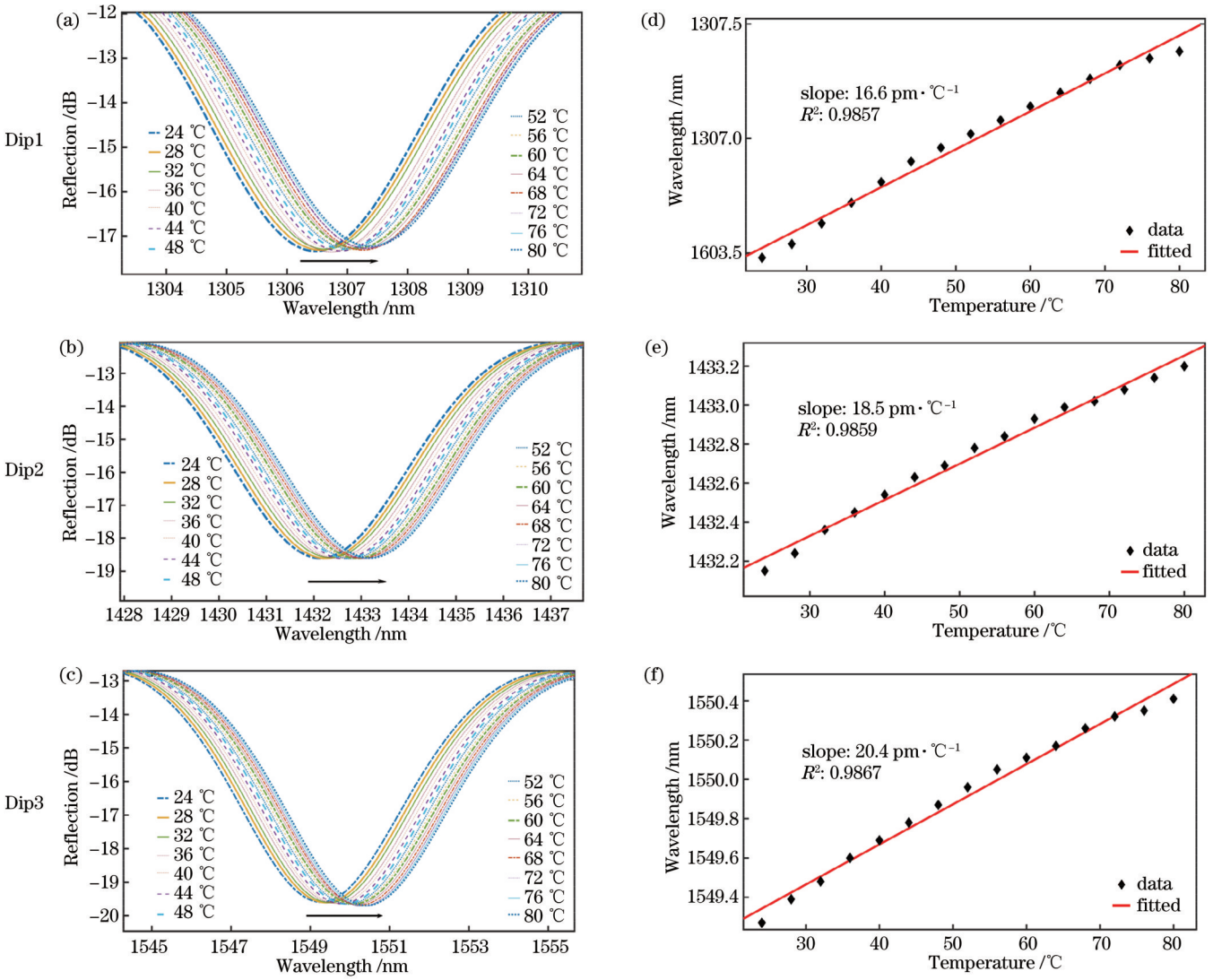


图 8　温度实验的反射光谱变化图与线性拟合图。(a)～(c)反射光谱变化图;(d)～(f)线性拟合图

Fig. 8　Reflectance spectrum variation diagram and linear fitting diagram of temperature experiment. (a)-(c) Reflection spectrum variation diagram; (d)-(f) linear fitting diagram

式中:$\Delta\varepsilon$为应变变化量;$\Delta H$为湿度变化量;$\Delta\lambda_1$、$\Delta\lambda_2$和$\Delta\lambda_3$为谐振波谷Dip1、Dip2和Dip3的中心波长偏移量;$K_{S_1}$、$K_{T_1}$和$K_{H_1}$分别为波谷Dip1的应变灵敏系数、温度灵敏系数和湿度灵敏系数;$K_{S_2}$、$K_{T_2}$和$K_{H_2}$分别为波谷Dip2的应变灵敏系数、温度灵敏系数和湿度灵敏系数;$K_{S_3}$、$K_{T_3}$和$K_{H_3}$分别为波谷Dip3的应变灵敏系数、温度灵敏系数和湿度灵敏系数。由式(11)可得,波谷Dip1、Dip2和Dip3的应变、温度和湿度与中心波长漂移量的关系为

$$\begin{bmatrix}\Delta\lambda_1\\ \Delta\lambda_2\\ \Delta\lambda_3\end{bmatrix}=\begin{bmatrix}K_{S_1} & K_{T_1} & K_{H_1}\\ K_{S_2} & K_{T_2} & K_{H_2}\\ K_{S_3} & K_{T_3} & K_{H_3}\end{bmatrix}\begin{bmatrix}\Delta\varepsilon\\ \Delta T\\ \Delta H\end{bmatrix}。\tag{12}$$

对式(12)求逆可得应变、温度和湿度的微小变量,即

$$\begin{bmatrix}\Delta\varepsilon\\ \Delta T\\ \Delta H\end{bmatrix}=\begin{bmatrix}K_{S_1} & K_{T_1} & K_{H_1}\\ K_{S_2} & K_{T_2} & K_{H_2}\\ K_{S_3} & K_{T_3} & K_{H_3}\end{bmatrix}^{-1}\begin{bmatrix}\Delta\lambda_1\\ \Delta\lambda_2\\ \Delta\lambda_3\end{bmatrix}。\tag{13}$$

若已测得该光纤传感器对应变、温度和湿度变化的灵敏度,即可利用光谱仪监测反射谱三个波谷中心波长的变化。将实验结果代入式(13)中可求得应变、温度和湿度的变化量,相应的公式为

$$\begin{bmatrix}\Delta\varepsilon\\ \Delta T\\ \Delta H\end{bmatrix}=\begin{bmatrix}4.0 & 16.6 & 12.6\\ 4.3 & 18.5 & 13.5\\ 4.8 & 20.4 & 14.6\end{bmatrix}^{-1}\begin{bmatrix}\Delta\lambda_1\\ \Delta\lambda_2\\ \Delta\lambda_3\end{bmatrix},\tag{14}$$

对式(14)求解逆矩阵可得

$$\begin{bmatrix}\Delta\varepsilon\\ \Delta T\\ \Delta H\end{bmatrix}=\begin{bmatrix}4.15 & -11.50 & 7.05\\ -1.58 & 1.63 & -0.14\\ 0.85 & 1.50 & -2.05\end{bmatrix}\begin{bmatrix}\Delta\lambda_1\\ \Delta\lambda_2\\ \Delta\lambda_3\end{bmatrix},\tag{15}$$

在式(15)中代入波长偏移量可直接求得应变、温度和湿度的变化。

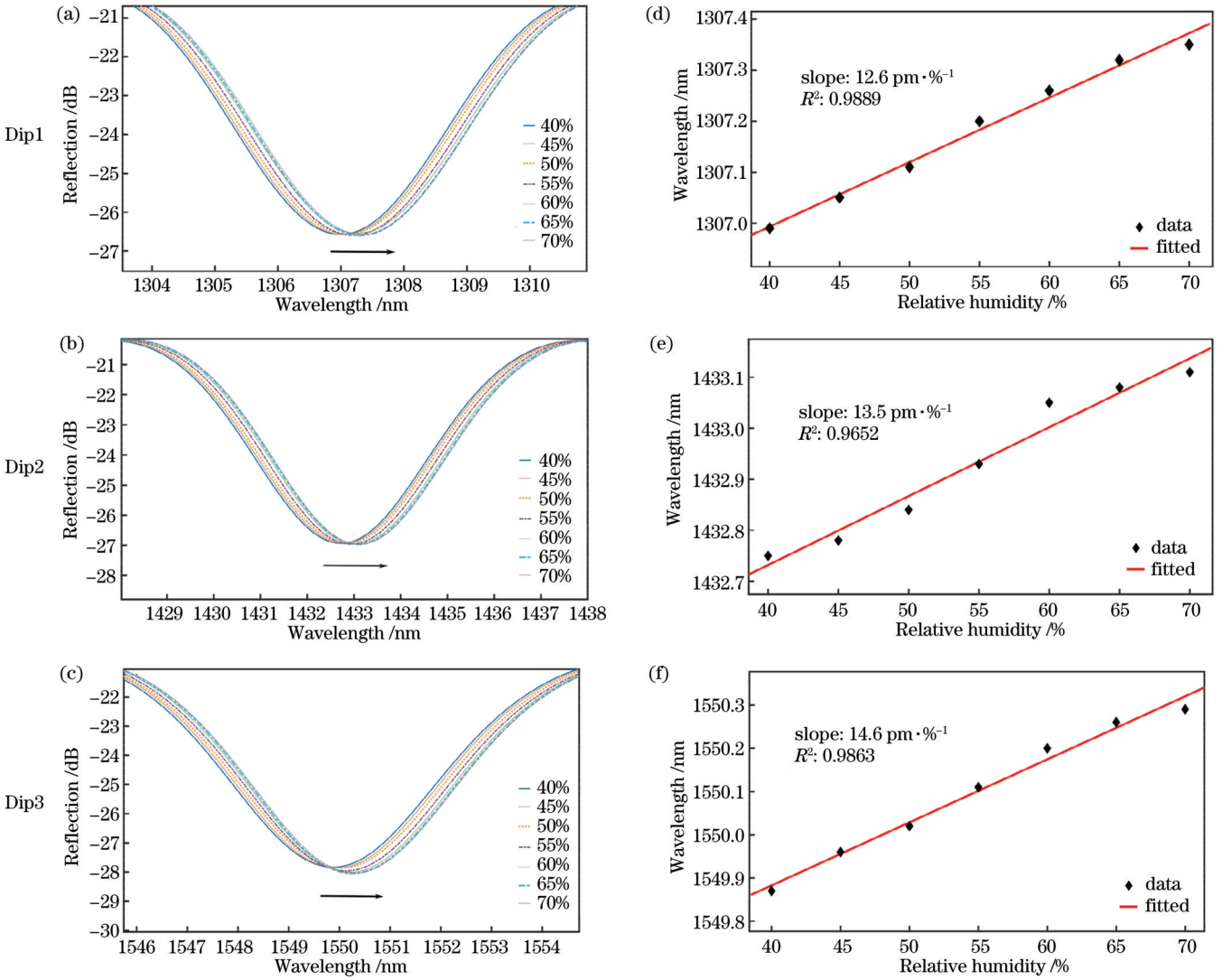


图 9　湿度实验的反射光谱变化图与线性拟合图。(a)～(c)反射光谱变化图;(d)～(f)线性拟合图

Fig. 9　Reflectance spectrum variation diagram and linear fitting diagram of humidity experiment. (a)-(c) Reflection spectrum variation diagram; (d)-(f) linear fitting diagram

## 4　结　　论

运用飞秒激光划线和光纤熔接机放电制作了MZI与FPI级联的光纤传感器,并通过实验验证了它的三参量传感特性。传感器在三个波谷处的应变灵敏度分别为 4.0 pm/με、4.3 pm/με、4.8 pm/με,灵敏度相对较高,量程为 600 με。在未涂覆 GQDs-PVA 时,传感器的温度和湿度灵敏度几乎为 0。涂覆 GQDs-PVA 到器件的锥部后进行温度和湿度实验,可以发现:三个波谷处的温度灵敏度分别为 16.6 pm/℃、18.5 pm/℃、20.4 pm/℃,温度的测量范围为 24～80 ℃;三个波谷处的相对湿度灵敏度分别为 12.6 pm/%、13.5 pm/%、14.6 pm/%,可测相对湿度范围为 40%～70%;应力、温度、湿度均与对应的中心波长有良好的线性关系。最后,构建三阶矩阵以消除交叉敏感,实现了应力、温度、湿度的同时测量。所提传感器制作简单、灵敏度高,在医疗监测、食品安全和环境检测等领域中均具有良好的应用前景。

## 参　考　文　献

[1] Roriz P, Silva S, Frazão O, et al. Optical fiber temperature sensors and their biomedical applications[J]. Sensors, 2020, 20(7): 2113.

[2] Joe H E, Yun H, Jo S H, et al. A review on optical fiber sensors for environmental monitoring[J]. International Journal of Precision Engineering and Manufacturing-Green Technology, 2018, 5(1): 173-191.

[3] Chen M Q, Zhao Y, Xia F, et al. High sensitivity temperature sensor based on fiber air-microbubble Fabry-Perot interferometer with PDMS-filled hollow-core fiber[J]. Sensors and Actuators A: Physical, 2018, 275: 60-66.

[4] 胡白燕, 文富荣, 程永山, 等. 基于级联腔法布里-珀罗干涉仪的温度和压力同时测量[J]. 激光与光电子学进展, 2021, 58(19): 1906006.
Hu B Y, Wen F R, Cheng Y S, et al. Simultaneous measurement of temperature and pressure based on cascaded Fabry-Perot interferometer[J]. Laser & Optoelectronics

Progress, 2021, 58(19): 1906006.

[5] Bhardwaj V, Kishor K, Sharma A C. Tapered optical fiber geometries and sensing applications based on Mach-Zehnder Interferometer: a review[J]. Optical Fiber Technology, 2020, 58: 102302.

[6] 徐妍妍, 李俊, 李浩, 等. 基于拉锥七芯光纤的湿度传感器研究[J]. 中国激光, 2021, 48(23): 2306002.
Xu Y Y, Li J, Li H, et al. Research on humidity sensor based on tapered seven core fiber[J]. Chinese Journal of Lasers, 2021, 48(23): 2306002.

[7] Liu S, Wang Y P, Liao C R, et al. High-sensitivity strain sensor based on in-fiber improved Fabry-Perot interferometer[J]. Optics Letters, 2014, 39(7): 2121-2124.

[8] Dong L G, Gang T T, Bian C, et al. A high sensitivity optical fiber strain sensor based on hollow core tapering[J]. Optical Fiber Technology, 2020, 56: 102179.

[9] Dong X R, Du H F, Sun X Y, et al. A novel strain sensor with large measurement range based on all fiber Mach-Zehnder interferometer[J]. Sensors, 2018, 18(5): 1549.

[10] 孙萌萌, 葛益娴, 沈令闻, 等. 基于电弧放电优化的光纤法珀湿度传感器[J]. 光学学报, 2022, 42(10): 1006002.
Sun M M, Ge Y X, Shen L W, et al. Optical fiber Fabry-Perot humidity sensor based on arc discharge optimization[J]. Acta Optica Sinica, 2022, 42(10): 1006002.

[11] Gao H, Hu H F, Zhao Y, et al. Highly-sensitive optical fiber temperature sensors based on PDMS/silica hybrid fiber structures[J]. Sensors and Actuators A: Physical, 2018, 284: 22-27.

[12] Chen N, Zhou X, Li X G. Highly sensitive humidity sensor with low-temperature cross-sensitivity based on a polyvinyl alcohol coating tapered fiber[J]. IEEE Transactions on Instrumentation and Measurement, 2021, 70: 9503308.

[13] Hernaez M, Acevedo B, Mayes A G, et al. High-performance optical fiber humidity sensor based on lossy mode resonance using a nanostructured polyethylenimine and graphene oxide coating[J]. Sensors and Actuators B: Chemical, 2019, 286: 408-414.

[14] Li J X, Tong Z R, Jing L, et al. Fiber temperature and humidity sensor based on photonic crystal fiber coated with graphene oxide [J]. Optics Communications, 2020, 467: 125707.

[15] Fu H Y, Zhang S W, Chen H, et al. Graphene enhances the sensitivity of fiber-optic surface plasmon resonance biosensor[J]. IEEE Sensors Journal, 2015, 15(10): 5478-5482.

[16] Gao X G, Cheng L X, Jiang W S, et al. Graphene and its derivatives-based optical sensors[J]. Frontiers in Chemistry, 2021, 9: 615164.

[17] Luo J J, Liu G S, Zhou W J, et al. A graphene-PDMS hybrid overcoating enhanced fiber plasmonic temperature sensor with high sensitivity and fast response[J]. Journal of Materials Chemistry C, 2020, 8(37): 12893-12901.

[18] Guo Y Y, Han B, Du J T, et al. Kilometers long graphene coated optical fibers for fast thermal sensing[J]. Research, 2021, 2021: 5612850.

[19] Zhao Y, Li X G, Zhou X, et al. Review on the graphene based optical fiber chemical and biological sensors[J]. Sensors and Actuators B: Chemical, 2016, 231: 324-340.

[20] Lü C, Hu C, Luo J H, et al. Recent advances in graphene-based humidity sensors[J]. Nanomaterials, 2019, 9(3): 422.

[21] Kumar Y R, Deshmukh K, Sadasivuni K K, et al. Graphene quantum dot based materials for sensing, bio-imaging and energy storage applications: a review[J]. RSC Advances, 2020, 10(40): 23861-23898.

[22] Zhao Y, Tong R J, Chen M Q, et al. Fluorescence temperature sensor based on GQDs solution encapsulated in hollow core fiber [J]. IEEE Photonics Technology Letters, 2017, 29(18): 1544-1547.

[23] Zhao Y, Tong R J, Chen M Q, et al. Relative humidity sensor based on hollow core fiber filled with GQDs-PVA[J]. Sensors and Actuators B: Chemical, 2019, 284: 96-102.

[24] Wang N, Tian W H, Zhang H S, et al. An easily fabricated high performance Fabry-Perot optical fiber humidity sensor filled with graphene quantum dots[J]. Sensors, 2021, 21(3): 806.

[25] 刘靖阳, 王涛, 张倩, 等. BOTDA系统温度应变双参量传感技术研究进展[J]. 激光与光电子学进展, 2021, 58(13): 1306021.
Liu J Y, Wang T, Zhang Q, et al. Research progress on temperature-strain dual-parameter sensing in BOTDA system [J]. Laser & Optoelectronics Progress, 2021, 58(13): 1306021.

[26] Li X G, Nguyen L V, Becker M, et al. Simultaneous measurement of temperature and refractive index using an exposed core microstructured optical fiber[J]. IEEE Journal of Selected Topics in Quantum Electronics, 2020, 26(4): 5600107.

[27] 邓理, 张建奇, 孙浩, 等. 基于静电纺丝纳米纤维膜的光纤温湿度传感器[J]. 激光与光电子学进展, 2021, 58(9): 0906006.
Deng L, Zhang J Q, Sun H, et al. Optical fiber temperature and humidity sensor based on film prepared by electrospinning nanofibers[J]. Laser & Optoelectronics Progress, 2021, 58(9): 0906006.

[28] Chen N, Liu C N, Lu Z Q, et al. Femtosecond laser processing for a high sensitivity fiber MZI microcavity[J]. Optics Express, 2022, 30(8): 12397-12408.

[29] Abbas L G, Ai Z, Mumtaz F, et al. Temperature and strain sensing with hybrid interferometer[J]. IEEE Sensors Journal, 2021, 21(23): 26785-26792.

[30] Chen M Q, Zhao Y, Wei H M, et al. Cascaded FPI/LPFG interferometer for high-precision simultaneous measurement of strain and temperature[J]. Optical Fiber Technology, 2019, 53: 102025.

[31] Xiong M L, Gong H P, Qian Z H, et al. Simultaneous measurement of liquid level and temperature based on spherical-shape structures and long period fiber grating[J]. Sensors and Actuators A: Physical, 2016, 239: 196-200.

[32] Liu F L, Zhang Y M, Meng F Y, et al. Complex optical fiber sensor based on the Vernier effect for temperature sensing[J]. Optical Fiber Technology, 2021, 61: 102424.

[33] Liu G G, Han M, Hou W L. High-resolution and fast-response fiber-optic temperature sensor using silicon Fabry-Pérot cavity [J]. Optics Express, 2015, 23(6): 7237-7247.

# Fiber Optic Sensor for Simultaneous Measurement of Three Parameters in FP Cavity and MZI Cascade

Peng Min, Lu Zhiqi, Liu Changning*

*College of Physics and Electronic Science, Hubei Normal University, Huangshi* 435002, *Hubei, China*

## Abstract

**Objective** A multiparametric fiber optic sensor with a pull-tapered fiber modified by sensitive materials and a microcavity cascade is fabricated, and its strain, temperature, and humidity characteristics are experimentally demonstrated. The proposed microcavity is formed by a femtosecond laser scribing discharge and tapered. The interference peak of the reflection spectrum of the sensor is sensitive to the change in strain, and the experimental results show that the strain sensitivity is 4.8 pm/με, but the structure is insensitive to both temperature and humidity. After the tapered part of the structure is coated with polyvinyl alcohol (PVA) doped with graphene quantum dots (GQDs), the sensitivity of temperature and humidity is significantly improved, with the maximum temperature sensitivity of 20.4 pm/℃ and the maximum relative humidity sensitivity of 14.6 pm/%. Dip1, Dip2, and Dip3 are analyzed, and then the cross-sensitivity is eliminated by using a third-order matrix, so as to simultaneously measure strain, temperature, and humidity. The device is easily fabricated, and it has a small size, excellent linearity, and good application prospects.

**Methods** Firstly, the femtosecond laser pulse is focused on the single-mode fiber (SMF) with an OLYMPUS objective lens with a numerical aperture of 0.7, and the program is run to write the optical fiber core axially with a controlled writing length of 45 μm, and a fiber fusion splicer is used to discharge the fiber at the center of the inscription. The discharge current and the discharge time of the fusion splicer are set to 20 mA and 1500 ms, respectively, and the bubble is generated inside the fiber with a width of 82 μm and a length of 129 μm. Secondly, the SMF is tapered to obtain the Mach-Zehnder interferometer (MZI). The tapered area of the MZI is stretched to 277 μm, and the MZI is cascaded with a microbubble Fabry-Perot (FP) cavity to develop the required sensor device. The diameter of the tapered fiber after coating is 48 μm, and the coating thickness is 4 μm. 5 mg of GQDs and 100 mg of PVA are used, and they are mixed well, with 100 mL of pure water added. Then, the mixed solution is heated to 95 ℃ and stirred well by a magnetic stirrer for 1 h, so as to obtain the GQDs-PVA solution. After the solvent in the GQDs-PVA solution evaporates, a thin film attached to the tapered part of the sensor can be found, and its main components are PVA and GQDs. The film is observed under a scanning electron microscope, and the size and distribution of GQDs in the PVA film can be known. Finally, the initial spectrum of the sensor after coating GQDs-PVA is measured, and three resonance valleys, namely, Dip1, Dip2, and Dip3 are taken for observation and analysis.

**Results and Discussions** The temperature range of the experimental chamber is 20-100 ℃, with an accuracy of ±0.1 ℃, and the relative humidity measurement range is 10%-95%, with an accuracy of ±0.1%. The broadband light source is a spontaneous radiation source with a spectral range of 1250-1650 nm. The measurement range of the adopted optical spectrum analyzer is 600-1700 nm, with an accuracy of ±0.1 nm. The light is output from the broadband light source and transmitted to the sensor by the coupler. Then, the reflected light is transmitted back to the optical spectrum analyzer by the coupler. Dip1, Dip2, and Dip3 are selected to observe the spectral changes, and the temperature sensitivities are 16.6 pm/℃, 18.5 pm/℃, and 20.4 pm/℃, and the linearities are 0.9857, 0.9859, and 0.9867, respectively. The central wavelengths of Dip1, Dip2, and Dip3 have a positive linear relationship with humidity. The linearities are 0.9889, 0.9652, and 0.9863, and the relative humidity sensitivities are 12.6 pm/%, 13.5 pm/%, and 14.6 pm/%, respectively. The axial strain sensitivities are 4.0 pm/με, 4.3 pm/με, and 4.8 pm/με, and the linearities are 0.9993, 0.9995, and 0.9996, respectively. Finally, a third-order matrix is constructed to eliminate the cross-sensitivity between the three parameters.

**Conclusions** Optical fiber sensors cascaded by MZI and FPI are fabricated by femtosecond laser scribing and fiber fusion splicer discharge technology, and their three-parameter sensing characteristics are verified by experiments. The strain sensitivities at the three resonance valleys are 4.0 pm/με, 4.3 pm/με, and 4.8 pm/με, respectively, which are relatively high, with a range of 600 με. When GQDs-PVA is uncoated, the sensitivities of temperature and humidity of the sensor are almost zero. The temperature sensitivities at the three resonance valleys are 16.6 pm/℃, 18.5 pm/℃, and 20.4 pm/℃, and the measurement range of temperature is 24-80 ℃. The relative humidity sensitivities at the three resonance valleys are 12.6 pm/%, 13.5 pm/%, and 14.6 pm/%, and the measurable relative humidity range is

40%-70%. The strain, temperature, and humidity had a positive linear relationship with the corresponding central wavelength. Finally, the cross-sensitivity is eliminated by constructing a third-order matrix, and the strain, temperature, and humidity can be measured simultaneously. The proposed sensor can be easily fabricated, and it has high sensitivity and good application prospects in fields such as medical monitoring, food safety, and environmental detection.

**Key words** fiber optics; optical fiber sensors; strain; temperature; relative humidity; graphene quantum dots; polyvinyl alcohol